This is the accepted manuscript made available via CHORUS. The article has been published as:

Harmonic model of corrugations of incommensurate two-dimensional layers

Konrad Thürmer and Catalin D. Spataru

Phys. Rev. B **95**, 035432 — Published 30 January 2017

DOI: 10.1103/PhysRevB.95.035432

Harmonic model of corrugations of incommensurate 2D layers

Konrad Thürmer and Catalin D. Spataru

Sandia National Laboratories, Livermore, California 94550, USA

Abstract: We developed a method to predict the height corrugations of moiré structures resulting from varying azimuthal orientations of graphene on hexagonal boron nitride substrates. Our model accounts for the flexural rigidity of graphene and assumes a sinusoidal corrugation of the preferred height of C atoms above the substrate. Using 4 parameters derived from density functional theory (DFT) the model computes corrugations of incommensurate moiré structures currently inaccessible to DFT with an estimated accuracy on the order of 0.01 Å. We predict that azimuthally aligned graphene domains are energetically favored over rotated ones.

I. INTRODUCTION

Various properties of supported graphene films depend strongly on the exact positions of carbon atoms with respect to the underlying substrate [1,2]. Graphene ripples less than 1 nm high, for example, have been shown to cause spatial charge redistribution [3,4] and electron scattering [5], to enhance graphene's chemical reactivity [6,7], and affect its thermal stability [8,9]. Aiming for high-quality graphene electronics, the search for suitable substrates has increasingly focused on layered materials, like mica [10], hexagonal boron nitride (h-BN) [11], or MoS_2 [12]. Their strong intralayer and weak interlayer bonding allows preparation of large atomically flat substrates, which is a prerequisite for nearly defect free graphene heterostructures. Using h-BN substrates, Dean *et al.* [11] were able to fabricate graphene devices with carrier mobility and chemical reactivity nearly unaffected by defects. We expect the properties of such high-quality graphene heterostructures to be particularly sensitive to the sub-nanometer corrugations arising from the interaction between graphene and substrate lattices. Indeed, the moiré superlattices of graphene on BN have been implicated in the opening of an electronic gap at the Dirac point [13,14,15,16,17] and the emergence of electronic minibands [2,14,18], and are believed to affect optical [2,18] and magnetic properties [2].

Measuring the exact corrugation of atoms in graphene is exceedingly difficult [12,19,20,21], rendering impractical any experimental attempts to quantify how the structure varies with graphene's azimuthal orientation. And while density functional theory (DFT) can predict atom position in many systems, it cannot be applied straightforwardly to systems that are incommensurate or have large unit cells, such as graphene on a BN surface. Not

surprisingly, these difficulties led to large uncertainties regarding the exact atomic structure of graphene. Values reported for the corrugation of azimuthally aligned graphene on h-BN, for example, range from ~0.2 Å (predicted with DFT [15]) and ~0.4 Å (measured with Atomic Force Microscopy (AFM) [22]) to ~4 Å (apparent corrugation measured with Scanning Tunneling Microscopy (STM) [12]). We address these limitations by developing a simple moiré model with parameters derived from DFT calculations for systems strained into commensurate structures with manageable unit cell sizes (keeping graphene at the experimental lattice constant). Our moiré model, which takes into account the flexural rigidity of graphene and includes the influence of the substrate, is able to reproduce the DFT-relaxed carbon positions with an accuracy of < 0.01 Å. We then apply this model to the (realistic) unstrained C/BN system and predict how structure and energy vary with azimuthal orientation of the graphene sheet with respect to the h-BN substrate.

II. MOIRÉ CORRUGATION MODEL

The basic assumption of our model, adopted from an earlier model [9] for C/Ir(111), is the following: The carbon atoms' lateral positions are fixed to an ideal honeycomb lattice, thus neglecting any lateral relaxations. Their vertical positions relax until the forces due to carbon's interaction with the substrate F_{subs} are balanced by the vertical forces F_{flex} exerted by the neighboring C atoms due to graphene's flexural rigidity (see schematic in Fig.1(a)). Both types of forces are now, in contrast to the previous model [9], derived from DFT calculations. The new model also accounts for the two types of atoms, B and N, in the substrate.

We assume the preferred distance of the graphene sheet from the substrate to vary locally, depending only on the lateral position of the C atoms with respect to the substrate (for example, whether the C atom sits at an atop position, a threefold hollow site and so on). Here, the BN substrate is represented by a sum of sinusoids, each atom in the unit cell contributing with a set of 3 sinusoids. The B and N in-plane positions coincide with the maxima of each sinusoid set, respectively. The sum of all sinusoids yields the contour of minimum C-BN potential, i.e. the height z_{pref} where a C-atom would sit above BN in the absence of graphene flexural forces. Assuming a harmonic substrate-graphene interaction with a uniform spring constant (k_{inter}), the force F_{subs} on each C atom is proportional to how far the atom is displaced from its preferred height z_{pref}, i.e.,

$$F_{subs} = -k_{inter}(z - z_{pref}). \quad (1)$$

In the relaxed configuration, this force F_{subs} is balanced at each C atom by a force F_{flex} due to local bending of the graphene sheet. To compute F_{flex} acting on a given C atom, "atom 0", our model evaluates the bond angles of this C atom and the bond angles of its nearest neighbors. The model approximates that positioning atom 0 at a height h_0 above (or below if $h_0<0$) the

plane through its three nearest neighbors generates a force $-k_{flex}h_0$ acting on atom 0 and forces $k_{flex}h_0/3$ acting on each of its nearest neighbors (atoms 1, 2, and 3). Analogously, the height h_N of a nearest neighbor N (N=1,2,3) above its nearest neighbors contributes $-k_{flex}h_N$ to the flexural force F^{flex}_N acting on atom N, and $k_{flex}h_N/3$ acting on each of its nearest neighbors, one of which is atom 0. Adding these contributions, the flexural force on atom 0 becomes:

$$F^{flex}_0 = k_{flex}[-h_0 +(h_1+h_2+h_3)/3]. \quad (2)$$

This model does not require periodic boundary conditions and is therefore well suited for incommensurate systems. To suppress finite-size effects we evaluated systems containing 1000 x 1000 graphene unit cells. Model structures can be relaxed by straightforward iterations: Initially all C atoms are placed at their respective substrate-potential minima z_{pref}. Then half the C atoms (, e.g. sublattice A,) are shifted to heights at which F_{subs} and F_{flex} balance for those atoms. Then the second half of C atoms (sublattice B) moves to where F_{subs} and F_{flex} are balanced for them. Now the first half of C atoms has to move again to rebalance the forces etc.

III. ESTABLISHING MODEL PARAMETERS

The parameters of our model k_{flex}, k_{inter}, and the amplitudes A_B and A_N of the sinusoids representing B and N atoms of the substrate, are determined using dedicated DFT calculations described in paragraphs III. A and B. The lattice constant of unstrained BN is a_{BN}= 2.504 Å [23]; for unstrained supported graphene we use a_C= 2.46 Å, extracted from moiré patterns in STM images of incommensurate C/Ir(111)-R30° taken from Loginova *et al.*[24]. When graphene and BN are azimuthally aligned (, which we henceforth call “unrotated” or “R0°”), the moiré periodicity of the unstrained incommensurate system is 56.909 a_C= 55.909 a_{BN}= 140.0 Å. Accordingly, the least-strained commensurate structure places 57x57 graphene unit cells over 56x56 BN unit cells. Its unit cell contains 6498 C, 9408 B, and 9408 N atoms for 3 BN layers, which exceeds the size limit of current DFT implementations. Therefore, for most DFT computations we used a 15x15C/14x14BN (“15C/14BN”) instead, which is the least-strained (~5%) unrotated C/BN moiré structure that allowed structure relaxations with high precision at an acceptable timescale.

Our ab-initio calculations are based on Density Functional Theory (DFT) [25] within the local density approximation (LDA). It has been shown in the case of graphenic systems that LDA yields inter-layer equilibrium distances in excellent agreement with experiments and random-phase approximation (RPA) calculations [14,26,27]. The calculations were done with VASP [28] using projector augmented wave (PAW) [29] pseudopotentials and an energy cutoff of 500 eV. We have considered supercells with hundreds of atoms with one graphene layer on top of three hBN layers. Relaxation is allowed in graphene as well as two BN layers underneath, while the bottom BN layer is kept fixed. Calculations are run until all forces drop below 1 meV/Å.

We have checked the robustness of our model against van der Waals corrections and in-plane relaxations and found that they have little impact on the corrugation of graphene (see the Appendix).

A. Determining the spring constants k_{flex} and k_{inter}

To determine the spring constant k_{flex}, accounting for the flexural rigidity of graphene, we first generate a seed structure [30] by relaxing the 15C/14BN-R0° system with DFT. We then modify our seed structure by removing the BN substrate and iteratively shifting the C atoms until every C atom's position projected onto the plane through its nearest neighbors (NN) equals the center of mass of these NN. This generates a freestanding corrugated graphene layer with negligible lateral forces. Now, DFT is used to compute the forces on the C atoms with high precision, which are then fitted to the flexural forces according to Eq. (1), yielding the spring constant k_{flex}= 9.43 eV/Å^2. Fig. 1(b) shows that the forces computed with DFT can be fitted superbly well with formula (2) using just one universal parameter, k_{flex}.

To determine the spring constant k_{inter}, accounting for the graphene-BN interaction, we set up a 15C/14BN-R0° configuration in DFT, keep the BN substrate flat and fixed, and allow the graphene layer to relax (a similar value of k_{inter} is obtained if the graphene layer is flat). We then shift graphene vertically within z_{shift} =± 0.03 Å about the equilibrium position (the average height of graphene above BN is 3.38 Å) and fit the corresponding energy cost per C atom (computed with DFT) to $E_{subs} = k_{inter} z_{shift}^2/2$, yielding the value for the spring constant k_{inter}= 0.124 meV/Å^2(see Fig. 1(c)).

B. Determining the contour z_{pref} of preferred C–BN distance

To construct the contour of preferred C-BN distance, i.e. the preferred local C height z_{pref} above the BN substrate, we examine again the 15C/14BN-R0° system with DFT. We now evaluate the individual forces on each C atom for a graphene sheet constrained to be flat and roughly at its equilibrium distance from BN. The 3 BN layers used in the calculations were also kept at fixed positions and flat. Eq. (1) relates these computed forces (which we call "flat forces" or F_{flat}), to the preferred local height z_{pref} of C atoms above BN, for which we are seeking a simple but realistic expression in our model. The simplest possible way to represent the influence of a substrate with two types of atoms would be via two sets of three sinusoids:

$$\tilde{z}_{pref} = \sum_{i=1}^{3} [A_B \sin(\vec{G}_i \vec{r} + \varphi_B) + A_N \sin(\vec{G}_i \vec{r} + \varphi_N)] \qquad (3),$$

where indices B and N denote the substrate atom types B and N, respectively, and $\vec{G}_1 = \frac{2\pi}{a}(1,0)$, $\vec{G}_2 = \frac{2\pi}{a}\left(-\frac{\sqrt{3}}{2}, \frac{1}{2}\right)$, and $\vec{G}_3 = \frac{2\pi}{a}\left(-\frac{\sqrt{3}}{2}, -\frac{1}{2}\right)$, with "a" denoting the lattice constant of BN in the

interface plane. The phase factors φ_B and φ_N insure that the maxima of each set of sinusoids are above the B and N atoms' positions. The amplitudes A_B and A_N, representing the respective effect of B and N, are determined by evaluating the DFT forces on C atoms of flat graphene. To account for the finite size of the C-atom orbitals, an additional smearing procedure needs to be applied to the expression shown in Eq. (3). Based on our finding that in all examined LDA-relaxed structures the difference between the height of any C atom and the average height of its nearest neighbors is less than 0.0001 Å, we choose a simple smoothing procedure, namely averaging the values at each C atom and its nearest neighbors:

$$z_{pref}(C) = 0.5 * \tilde{z}_{pref}(C) + 0.5 * \frac{\tilde{z}_{pref}(C_{NN1})+\tilde{z}_{pref}(C_{NN2})+\tilde{z}_{pref}(C_{NN3})}{3}$$, and analogous for F_{flat} (4)

The two amplitudes A_B and A_N can be adjusted to fit the flat forces predicted by our moiré model (Eqs. 1, 3, and 4) to those computed with DFT. While the raw DFT forces can be directly used in the fit, we choose to smooth them out as well to reduce the effect of short-wavelength force components (higher G components than those included in eq. (3), which are not captured by our model and have little impact on the final relaxed structure). Fig. 1(d) shows that an excellent fit is obtained with A_N=0.161 Å and A_B=0.0234 Å. The positiveness of A_B and A_N reflects the fact that B atoms as well as N atoms exert upward repulsive forces on C atoms placed on top of them at heights equal or less than the average equilibrium C-BN distance. The larger weight on N atoms corresponds to their larger size compared to B atoms.

IV. TEST THE MOIRÉ MODEL'S ABILITY TO PREDICT STRUCTURE

In the previous section we have established our moiré model based on computed DFT forces. We now benchmark the model's capability to predict atomic positions of the graphene layer. In particular we test whether its 4 parameters derived from the 15C/14BN-R0° system are universal, i.e., applicable to arbitrary rotations of graphene versus the BN substrate. To allow comparisons with DFT the BN lattice has to be strained to obtain commensurate C/BN structures with supercell sizes still manageable by DFT. We examined rotations of graphene with respect to BN by 0°, 4.93°, 9.83°, 17.6°, and 30°, yielding the commensurate structures labeled R0°, R5°, R10°, R18°, and R30°. Except for the 15C/14BN R0° strained by ~5%, for the other four commensurate structures the BN lattice had to be strained by less than 1%.

Fig. 2 depicts these structures relaxed in our moiré model in comparison with configurations obtained in DFT (LDA). The color-coded top views of (a) and the line profiles in (b) both show the local height of the C atoms above the BN atoms at the C/BN interface. Strikingly, for all examined rotations, the top views of DFT and moiré model are almost indistinguishable! For a more quantitative comparison, Fig. 2(b) plots the local heights of all the C atoms in the respective C/BN unit cells, arranged zig-zag row by zig-zag row. Values for the root mean square difference Δz_{rms} between C atom heights predicted by DFT and the moiré

model are given below each line profile. The moiré model matches the DFT positions of the C atoms with a typical accuracy of Δz_{rms}<0.01 Å, which is remarkable given that only 4 non-adjustable parameters are used and kept constant for all rotations. Even for the R5°, which was reproduced with least accuracy, the position error is only Δz_{rms}=0.025 Å, and the profiles of DFT and moiré model share most structural details. The observation in DFT that the corrugation drops with increasing rotation angle is also reproduced well by our moiré model.

V. PREDICT STRUCTURE AND ENERGY OF UNSTRAINED C/BN MOIRÉS

We now apply our moiré model to more realistic unstrained C/BN systems, which due to their incommensurability are inaccessible to DFT, and predict their structure and energy for a variety of rotation angles. Since the validity of this model is not affected by incommensurability we expect its predictive capability established in the previous paragraph to carry over to unstrained moirés. Fig. 3(a) depicts how the unstrained C/BN moiré changes with increasing rotation angle. At 5° the lateral moiré periodicity has already decreased substantially, and continues to decrease monotonically until 30° of rotation. In addition to this well-known geometric effect, our model predicts in quantitative detail how structure and energy evolve with rotation (Fig. 3(b)). Separate model computations were performed for each of the 0.5° increments on model systems containing 1000 x 1000 graphene unit cells; and the structure relaxations were run until forces have dropped to less than 10^{-7} eV/Å per C atom.

Energy variations among differently oriented graphene sheets are expected to be small. They have been measured [9] for only one system, C/Ir(111), where they amount to less than 0.1 meV per C atom. In laterally-undistorted incommensurate moirés, all lateral positions of C atoms with respect to the substrate unit cell are occupied with equal probability, independent of the layer's orientation, suggesting an equal energy for all rotations (see also Ref.[31]). However, as proposed in Ref. [9] for C/Ir, a small energy difference might arise as a consequence of the graphene corrugation varying with rotation angle. In the next paragraph we will explore this argument in detail for the C/BN system.

The plots in Fig. 3(b) reveal that the graphene corrugation (black symbols, left y-axis) decreases monotonously with rotation angle, while the energy contributions from the C-BN interaction, E_{subs}, and the flexure of graphene, E_{flex}, exhibit a more complex behavior (blue symbols, right y-axis). Due to the small lattice mismatch between C and BN, at small rotation angles, the phase in the sinusoids of Eq. (3) and thus the preferred C-BN separation z_{pref} varies very little between neighboring C atoms. Therefore the graphene only has to bend very slightly for the C atoms to be near their preferred height z_{pref}. In fact, for the R0 the relaxation due to the bending rigidity barely affects the corrugation: it lowers it by just 0.1 % compared to the corrugation of the raw z_{pref} values. But as the rotation angle increases, the phase in the

sinusoids of Eq. (3) shifts more between NN C atoms, thus making the preferred C-BN separation z_{pref} oscillate with shorter wavelengths. Now the graphene sheet, attempting to place the C atoms near z_{pref}, has to bend more causing a rise in flexural energy E_{flex}. At 5°-10°, however, the wavelength of the z_{pref} oscillations (and the moiré period) become too small, exceeding the graphene sheet's ability to flex enough to follow the highly-curved substrate potential. As a consequence the C atoms are positioned farther away from their preferred location z_{pref}, which increases the C-BN interaction energy E_{subs} (open squares in Fig. 3(b)) and simultaneously reduces the graphene corrugation amplitude. Eventually, at around 9°, the reducing effect of shrinking corrugation on the flexural energy E_{flex} surpasses the enhancing effect of shorter moiré periods, and E_{flex} (open circles in Fig. 3(b)) starts the decline. For rotations larger than ~20° the graphene is essentially flat and located near the average of the preferred C-BN distance z_{pref}. The plot of E_{subs} shows a subtle drop at angles larger than 20°, which may be affected by the limitations of this model at very short moiré periods[32]. We note that including in-plane relaxations, which are not part of this model, might affect whether there is a local energy minimum at 30°. Nevertheless, we are confident that the model correctly predicts the energetic preference for small rotation angles, given that our computed values of the energy cost of rotating graphene on BN, ~0.3 meV/per C atom, is reasonably close to values of ~0.1meV/atom measured for C/Ir(111) [9].

VI. DETERMINE ABSOLUTE CORRUGATIONS OF C/BN

Our moiré model applies, strictly speaking, only to the relative local height of the C atoms above the nearby atoms of the substrate top layer. Absolute height and corrugation of graphene, however, are expected to differ slightly from the relative values due to some graphene-induced corrugation of the top substrate layer. In the 15C/14BN-R0° system, which we have explored extensively with DFT to extract the parameters for our moiré model, we observe that the BN top layer largely follows the graphene corrugation, albeit attenuated. This simple relationship between the height of the C atoms and the substrate atoms below suggests the possibility to use a corrugated BN top layer (instead of a flat one) in the DFT calculations dedicated to extract the moiré model parameters, and use those parameters to predict the absolute C heights of the unrotated R0° system [33].

To explore this possibility we applied the procedures described in section III, but replaced the flat BN top layer with corrugated BN. The plot in Fig. 4(a) shows, for example, that the DFT forces on flat graphene can be matched very well by fitting A_N and A_B of the moiré model, yielding A_N^{abs}=0.1929 Å and A_B^{abs}=0.0283 Å. (The spring constant for C-BN interaction as well as the flexural rigidity of graphene remain unchanged.) We now use these new parameters to predict the absolute corrugation of the 15C/14BN-R0° system. Comparisons of the top views in Fig. 4(b) and height profiles in Fig. 4(c) reveal that the modified parameter set

[A_N^{abs}, A_B^{abs}] yields an excellent match between moiré-model and DFT prediction: the root mean square height difference between the two is only 0.0042 Å, corroborating the ability of our model to predict absolute corrugations of unrotated C/BN structures.

We now apply our model to the realistic 57C/56BN-R0° system, which has the experimentally observed [12,18,22] moiré-cell size of 14 nm. Fig. 4(d) shows a top view of this system relaxed in our moiré model, and Fig. 4(e) the corresponding height profile. (An almost identical structure is obtained when we base our model parameters on DFT calculations that include semi-empirical van der Waals corrections via the DFT-D2 method [34], see Appendix A). We find an absolute corrugation of 0.43 Å, which agrees well with AFM measurements of Yang *et al*. (see height profile of Fig. 2(b) in Ref.[22]). Fig. 4(d) also illustrates how the lateral positions of the C atoms with respect to the BN top layers relate to the absolute height of the C atoms. The graphene protrusions are located where all the C atoms sit either on top of a B atom or a N atom. Depressions are found where half the C atoms rest on top of B atoms, the other half have no substrate top layer atom beneath, and the substrate top layer nitrogens sit below the centers of the graphene-honeycomb rings. The rounded topography, which lacks any sharp features, agrees well with Yankowitz *et al.'*s [35] finding that narrow moiré-cell boundaries are only observed in their experiments when graphene is pushed towards the BN substrate by an STM tip.

VII. Summary

We have shown that a 4-parameter moiré model can predict the atomic structure of graphene on BN with an estimated accuracy of ≈0.01 Å, relative to DFT. This remarkable accuracy suggests that the graphene corrugations are determined largely by simple harmonic interactions captured in our model. Our model predicts for the first time the graphene structure and energy for arbitrary azimuthal orientation relative to BN substrate. For azimuthally aligned C/BN we find a corrugation of 0.4 Å in agreement with previous AFM measurements [22]. Since the model is computationally cheap and does not require periodic boundary conditions, it can be applied to large unit cells or incommensurate systems inaccessible to DFT, e.g., unstrained C/BN-R0°. This property makes it straightforward to examine how graphene structure varies with rotation angle. For C/BN we predict that well aligned graphene, with rotation angles <3°, are energetically preferred by ≈0.3 meV per C atom over highly rotated (>15°) graphene sheets, presumable facilitating experimentally observed single-domain epitaxy [22]. We expect this moiré model to be transferrable to other system, where graphene is supported by atomically-flat single-crystalline substrates.

Acknowledgements

We thank Thomas Beechem for supporting this work and Norm Bartelt for insightful comments. This work was supported by the Sandia Laboratory Directed Research and Development (LDRD) Program. Sandia National Laboratories is a multi-program laboratory managed and operated by Sandia Corporation, a wholly owned subsidiary of Lockheed Martin Corporation, for the U.S. Department of Energy's National Nuclear Security Administration under contract DE-AC04-94AL85000.

APPENDIX

A. IMPACT OF VAN DER WAALS CORRECTIONS ON GRAPHENE CORRUGATION

Standard local and semilocal density functionals cannot capture correctly van der Waals interactions which may play an important role in layered materials. There are several methods to add van der Waals corrections within DFT. We choose the DFT-D2 method in the semi-empirical form of Grimme ("vdW-Grimme") [34] to examine the impact of van der Waals corrections on computed graphene corrugations. We performed a parameterization analogous to sections III A. and B. and section VI, choosing vdW-Grimme instead of LDA for the required DFT calculations. We obtain the parameters A_N^{abs}= 0.1922 Å, A_B^{abs}= 0.0382 Å, and k_{inter}^{abs}= 0.187 meV/Å^2. Using these parameters our moiré model predicts the absolute graphene corrugation for the 15C/14BN-R0° system (see Fig. 5(a)). The moiré model not only reproduces the corrugation of the DFT structure relaxed using vdW-Grimme; it's corrugations also agree very well with those of the structure relaxed with DFT-LDA and the LDA-based moiré model.

We then compared the absolute corrugations of the unstrained 57C/56BN-R0° system predicted with our moiré model based on parameters obtained with DFT-vdW-Grimme with those based on DFT-LDA (same data as discussed in section VI and shown in Fig. 4(e)). Both methods agree very well: the root mean square height difference between the two is only 0.0066 Å; and the maximum corrugations, 0.4331 Å for the LDA-based moiré prediction and 0.4318 Å for vdW-Grimme-based moiré parameters, are almost equal.

While there are many other methods that can include van der Waals corrections, the very good agreement between LDA and vdW-Grimme for the computed corrugations in commensurate C-BN systems gives us confidence that our model is robust and van der Waals corrections should not have a major impact on the predicted incommensurate moiré structures.

B. FRENKEL-KONTOROVA MODEL

To test whether the structure of the 57C/56BN-R0° system is significantly affected by in-plane relaxations, which so far have been excluded from our moiré model, we performed Frenkel-Kontorova (FK) model calculations. With respect to the moiré model presented in detail above, we now include lateral components (along x and y directions) for the force acting on a C atom. This is done in two steps. First, to compute the forces generated within graphene alone, we augment the flexural force with a force $F^{\text{in-plane}}$ that arises when a C atom is shifted laterally away from the center of mass of its nearest neighbors. For the x-component of this lateral force acting on atom 0 we use $F^{\text{in-plane}}_0 = k_{\text{in-plane}}[-x_0 + (x_1+x_2+x_3)/3]$ (and similar for the y-component), where $k_{\text{in-plane}} = 61.6$ eV/Å is determined from ab initio DFT/LDA calculations. Second, we account for the lateral forces F^{lateral} that C-atoms experience (almost entirely due to the substrate) when they are relaxed along the z-direction but not along x and y (as is the case with the structures discussed previously). We do this via $F^{\text{lateral}} = -dV/dr$, where the potential is obtained as a sum over sinusoids similar to Eq. 3:

$$\tilde{V} = \sum_{i=1}^{3} [A_B^V \sin(\vec{G}_i\vec{r} + \varphi_B) + A_N^V \sin(\vec{G}_i\vec{r} + \varphi_N)] \quad (5)$$

A good fit to the LDA lateral forces calculated for the 1C/1BN-R0° structure (for a dense grid of relative lateral shifts between graphene and BN) can be obtained with amplitudes $A_N^V = 4.9$ meV and $A_B^V = A_N^V/8$, and with a (slightly different) smoothing procedure:

$$V(C) = \frac{8}{11} * \tilde{V}(C) + \frac{3}{11} * \frac{\tilde{V}(C_{NN1}) + \tilde{V}(C_{NN2}) + \tilde{V}(C_{NN3})}{3} \quad (6)$$

We found an average in-plane relaxation of less than 0.05 Å and a maximum in-plane shift of 0.11 Å. These small displacements, compared to the BN lattice constant of 2.5 Å, have only a very subtle effect on the 57C/56BN-R0° structure (compare Fig.6(a) with Fig. 6(b)). They cause additional out-of-plane relaxation w.r.t. the moiré model discussed in section VI, leading to a root mean square height difference between the two of 0.014 Å and a reduction of the maximum corrugation from 0.433 Å to 0.427 Å. Within our LDA-based FK model we cannot find large commensurate domains (with periodicity of 14 nm) as suggested by recent AFM measurements in the PeakForce mode [13,16] and molecular dynamics simulations on rigid h-BN substrates [36]. Only when examining C/BN systems strained into an unrealistically large periodicity, such as the 148C/147BN-R0° with 37 nm periodicity considered by Jung *et al.* [14], one obtains contracted ridges (Fig. 6(c)) in agreement with Ref. [14]. Very recent work by Yankowitz *et al.* [35] suggests that sharp contracted ridges at small angles are in fact a tip-induced artifact, not an equilibrium property of the system, consistent with our lack of finding large commensurate domains.

Figure Captions

Fig. 1. The moiré model. **(a)** Schematic illustrating the balance of forces in the moiré model. The solid sinusoidal line represents the contour of minimum potential of the graphene-substrate interaction, which is the sum of contributions from B and N atoms (blue and green dotted lines). This interaction generates a force F_{subs} pulling atom 0 upwards, while the lower-lying nearest neighbor C atoms 1, 2, and 3 (not shown), pull atom 0 downwards (F_{flex}) due to the flexural rigidity of graphene. **(b)** Fit of the spring constant k_{flex} representing the flexural rigidity of graphene in the moiré model to match the (flexural) forces acting on the C atoms in freestanding corrugated graphene, computed with DFT for the 15C/14BN-R0° system. **(c)** Energy cost of shifting a relaxed graphene layer vertically with respect to flat and fixed BN, computed with DFT to extract the spring constant k_{inter} for the C-BN interaction. **(d)** Fit of the moiré model to the DFT forces acting on flat graphene due to the interaction with the (flat and fixed) BN substrate. Only two parameters, A_N and A_B representing the contributions of B and N atoms to the sinusoidal contour of minimum C-BN interaction potential, were adjusted. Forces are shown for all the C atoms in the 15C/14BN unit cell, arranged zig-zag row by zig-zag row.

Fig. 2. Comparison between DFT (LDA) and moiré-model predictions of various commensurate structures with different rotation angles. The local relative height of C atoms above the BN top layer is color-coded (representing the full range of local heights for each individual structure) in **(a)** and shown in the height profiles of **(b)**. These profiles show the local heights of all the C atoms in the respective C/BN unit cells, arranged zig-zag row by zig-zag row. Values for the root mean square difference Δz_{rms} between C atom heights predicted by DFT and the moiré model are given below each plot.

Fig. 3. Moiré-model predictions of unstrained C/BN at various rotations. **(a)** Top views of unstrained R0°, R5°, R15°, and R30°. **(b)** Plots of corrugation and energy as a function of rotation angle. The left y-axis and the symbols colored black show the corrugation, defined here as the maximum height difference, and the roughness, defined here as the root mean square deviation from the average C-BN separation. The right y-axis and the blue symbols show the energy per C atom due to the flexure of graphene (open circles) and the displacement of C atoms away from their preferred distance to the substrate (open squares). The total energy (filled circles) is the sum of the two contributions, which is lowest when graphene and BN are azimuthally aligned, i.e., for structures close to R0°.

Fig. 4. Absolute corrugations of the C/BN-R0° considering relaxation of the top BN layer. **(a)** Fit of the moiré model to the DFT forces acting on flat graphene due to the interaction with the corrugated BN substrate, used to extract A_N^{abs} and A_B^{abs}. **(b,c)** Comparison of the 15C/14BN-R0° predicted by the moiré model with the structure relaxed with DFT. The excellent agreement

suggests that the moiré model can accurately predict absolute corrugations of C/BN-R0° structures. **(d,e)** Moiré-model prediction for the absolute corrugation of the realistic unstrained 57C/56BN-R0° structure. Graphene is highest where all C atoms sit above B or N top layer atoms, and lowest where half the C atoms sit above B and the other half above centers of BN rings.

Fig. 5. (a) Comparison of the absolute corrugations of the 15C/14BN-R0° system computed with two DFT methods, DFT-LDA (blue line, same data as in Fig. 4(c)) and DFT-vdW-Grimme [34] (green), and predicted with the moiré model based on parameterization using DFT-vdW-Grimme (black) and DFT-LDA (red, same data as in Fig. 4(c)). The average C-atom height has been set to zero in all four cases.

(b) Absolute corrugations of the 57C/56BN-R0° system predicted with our moiré model based on parameters obtained with DFT-LDA (red, same data as shown in Fig. 4(e)) and DFT-vdW-Grimme (black, same parameters as in Fig. 5(a)).

Fig. 6: Top views comparing **(a)** 57C/56BN-R0° structure predicted by the moiré model without in-plane relaxation (same as Fig. 4(d), **(b)** 57C/56BN-R0° structure laterally-relaxed using a Frenkel-Kontorova model, **(c)** 148C/147BN-R0° structure with unrealistically large moiré periodicity (37 nm), relaxed in a Frenkel-Kontorova model, reproducing the contracted ridges reported by Jung *et al.* [14]. In (a), (b), and (c), 2 x 2 moiré cells are shown, and the color scale representing the graphene corrugation spans 0.43 Å.

[1] S. Deng, V. Berry, Wrinkled, rippled and crumpled graphene: an overview of formation mechanism, electronic properties, and applications. *Mater. Today* **19**, 197 (5//, 2016), and references therein.

[2] J. R. Wallbank, M. Mucha-Kruczynski, X. Chen, V. I. Fal'ko, Moire superlattice effects in graphene/boron-nitride van der Waals heterostructures. *Ann Phys-Berlin* **527**, 359 (Jun, 2015), and references therein.

[3] A. L. Vázquez de Parga *et al.*, Periodically Rippled Graphene: Growth and Spatially Resolved Electronic Structure. *Phys. Rev. Lett. (USA)* **100**, 056807 (02/07/, 2008).

[4] L. Brey, J. J. Palacios, Exchange-induced charge inhomogeneities in rippled neutral graphene. *Phys. Rev. B* **77**, 041403 (01/04/, 2008).

[5] M. I. Katsnelson, A. K. Geim, Electron Scattering on Microscopic Corrugations in Graphene. *Philosophical Transactions: Mathematical, Physical and Engineering Sciences* **366**, 195 (2008).

[6] A. T. N'Diaye, S. Bleikamp, P. J. Feibelman, T. Michely, Two-Dimensional Ir Cluster Lattice on a Graphene Moiré on Ir(111). *Phys. Rev. Lett. (USA)* **97**, 215501 (11/20/, 2006).

[7] X. Fan, R. Nouchi, K. Tanigaki, Effect of Charge Puddles and Ripples on the Chemical Reactivity of Single Layer Graphene Supported by SiO2/Si Substrate. *The Journal of Physical Chemistry C* **115**, 12960 (2011/07/07, 2011).

[8] E. Miniussi *et al.*, Thermal Stability of Corrugated Epitaxial Graphene Grown on Re(0001). *Phys. Rev. Lett. (USA)* **106**, 216101 (05/25/, 2011).

[9] P. C. Rogge *et al.*, Real-time observation of epitaxial graphene domain reorientation. *Nature Communications* **6**, 6880 (Apr, 2015).
[10] C. H. Lui, L. Liu, K. F. Mak, G. W. Flynn, T. F. Heinz, Ultraflat graphene. *Nature (UK)* **462**, 339 (11/19/print, 2009).
[11] C. R. Dean *et al.*, Boron nitride substrates for high-quality graphene electronics. *Nat Nano* **5**, 722 (10//print, 2010).
[12] C. P. Lu, G. H. Li, K. Watanabe, T. Taniguchi, E. Y. Andrei, MoS2: Choice Substrate for Accessing and Tuning the Electronic Properties of Graphene. *Phys. Rev. Lett. (USA)* **113**, (Oct, 2014).
[13] C. R. Woods *et al.*, Commensurate-incommensurate transition in graphene on hexagonal boron nitride. *Nat. Phys.* **10**, 451 (2014).
[14] J. Jung, A. M. DaSilva, A. H. MacDonald, S. Adam, Origin of band gaps in graphene on hexagonal boron nitride. *Nat Commun* **6**, (02/19/online, 2015).
[15] M. Bokdam, T. Amlaki, G. Brocks, P. J. Kelly, Band gaps in incommensurable graphene on hexagonal boron nitride. *Phys. Rev. B* **89**, 201404 (05/19/, 2014).
[16] P. San-Jose, A. Gutiérrez-Rubio, M. Sturla, F. Guinea, Spontaneous strains and gap in graphene on boron nitride. *Phys. Rev. B* **90**, 075428 (2014).
[17] M. Neek-Amal, F. M. Peeters, Graphene on hexagonal lattice substrate: Stress and pseudo-magnetic field. *Appl. Phys. Lett.* **104**, 173106 (2014).
[18] G. X. Ni *et al.*, Plasmons in graphene moire superlattices. *Nat. Mater.* **14**, 1217 (Dec, 2015).
[19] Z. Sun *et al.*, Topographic and electronic contrast of the graphene moiré on Ir(111) probed by scanning tunneling microscopy and noncontact atomic force microscopy. *Phys. Rev. B* **83**, 081415 (02/25/, 2011).
[20] C. Busse *et al.*, Graphene on Ir(111): Physisorption with Chemical Modulation. *Phys. Rev. Lett. (USA)* **107**, 036101 (07/13/, 2011).
[21] T. A. Land, T. Michely, R. J. Behm, J. C. Hemminger, G. Comsa, STM investigation of single layer graphite structures produced on Pt(111) by hydrocarbon decomposition. *Surf. Sci. (Netherlands)* **264**, 261 (1992/03/15, 1992).
[22] W. Yang *et al.*, Epitaxial growth of single-domain graphene on hexagonal boron nitride. *Nat. Mater.* **12**, 792 (Sep, 2013).
[23] R. W. Lynch, H. G. Drickamer, Effect of high pressure on lattice parameters of diamond graphite and hexagonal boron nitride. *J. Chem. Phys. (USA)* **44**, 181 (1966).
[24] E. Loginova, S. Nie, K. Thürmer, N. C. Bartelt, K. F. McCarty, Defects of graphene on Ir(111): Rotational domains and ridges. *Phys. Rev. B* **80**, 085430 (Aug, 2009).
[25] W. Kohn, L. J. Sham, Self-Consistent Equations Including Exchange and Correlation Effects. *Physical Review* **140**, A1133 (11/15/, 1965).
[26] T. Gould, S. Lebegue, J. F. Dobson, Dispersion corrections in graphenic systems: a simple and effective model of binding. *J. Phys.-Condes. Matter* **25**, (Nov, 2013).
[27] J. Jung, A. Raoux, Z. H. Qiao, A. H. MacDonald, Ab initio theory of moire superlattice bands in layered two-dimensional materials. *Phys. Rev. B* **89**, (May, 2014).
[28] G. Kresse, D. Joubert, From ultrasoft pseudopotentials to the projector augmented-wave method. *Phys. Rev. B* **59**, 1758 (Jan, 1999).
[29] P. E. Blochl, Projector augmented-wave method. *Phys. Rev. B* **50**, 17953 (Dec, 1994).
[30] Crude “seed structures” needed for model parameterization were obtained with computationally-cheap low-precision DFT relaxations. Time-consuming high-precision DFT structure relaxations were only performed later to benchmark the accuracy of our moiré model using commensurate test structures.

[31] F. Grey, J. Bohr, A Symmetry Principle for Epitaxial Rotation. *EPL (Europhysics Letters)* **18**, 717 (1992).
[32] These short-wavelength structures can be affected by the inclusion of in-plane relaxations or the smoothing choice for the substrate potential. Also the model had been parameterized using the longer-wavelength 15C/14BN structure.
[33] Predicting absolute height for different rotations would require a systematic DFT study of how the relationship between graphene corrugation and BN top layer corrugation evolves with rotation angle, which is beyond the scope of this work.
[34] S. Grimme, Semiempirical GGA-type density functional constructed with a long-range dispersion correction. *Journal of Computational Chemistry* **27**, 1787 (Nov, 2006).
[35] M. Yankowitz, K. Watanabe, T. Taniguchi, P. San-Jose, B. J. LeRoy, Pressure-induced commensurate stacking of graphene on boron nitride. *Nature Communications* **7**, (2016).
[36] M. M. van Wijk, A. Schuring, M. I. Katsnelson, A. Fasolino, Moiré Patterns as a Probe of Interplanar Interactions for Graphene on h-BN. *Phys. Rev. Lett.* **113**, 135504 (2014).

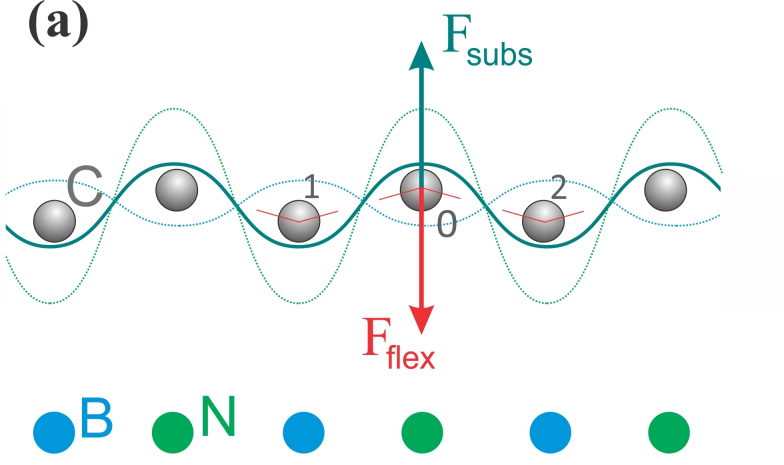
(a)
F subs
C
1
0
2
F flex
B
N

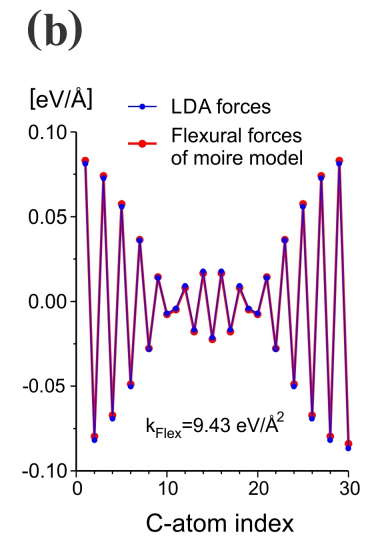
(b)
[eV/Å]
LDA forces
Flexural forces of moire model
0.10
0.05
0.00
-0.05
-0.10
k Flex=9.43 eV/Å2
0
10
20
30
C-atom index

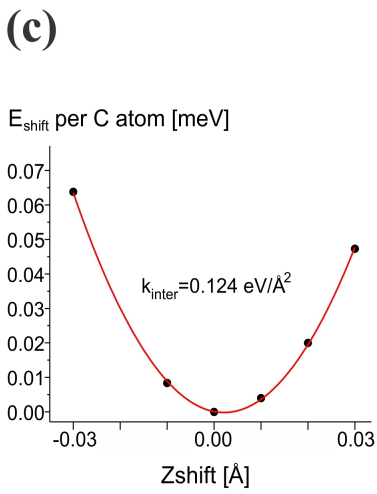
(c)
E shift per C atom [meV]
0.07
0.06
0.05
0.04
0.03
0.02
0.01
0.00
k inter=0.124 eV/Å2
-0.03
0.00
0.03
Zshift [Å]

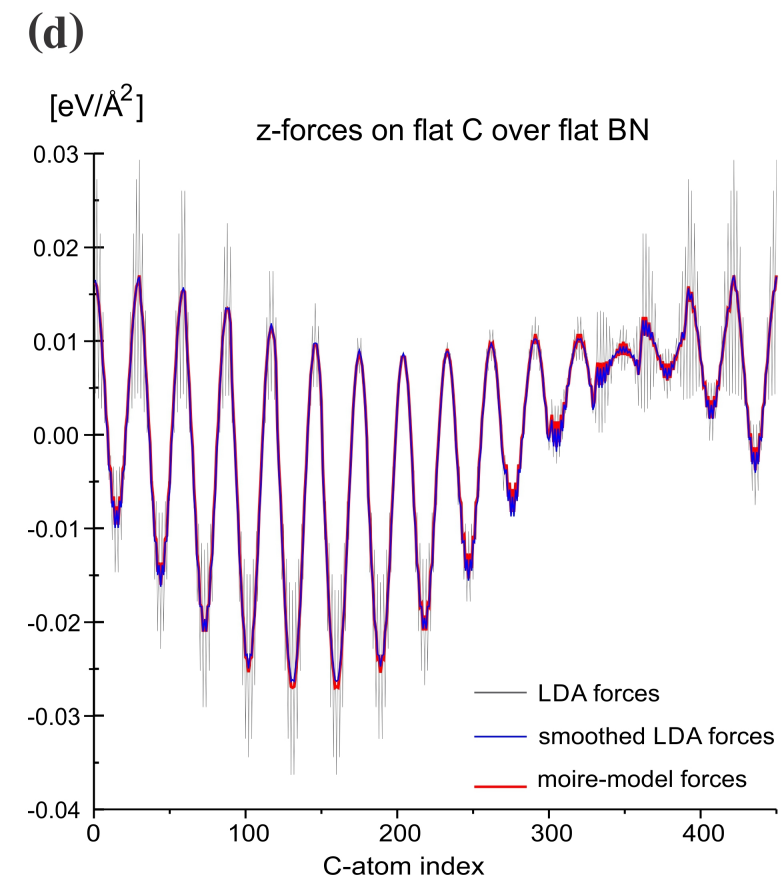
(d)
[eV/Å2]
z-forces on flat C over flat BN
0.03
0.02
0.01
0.00
-0.01
-0.02
-0.03
-0.04
LDA forces
smoothed LDA forces
moire-model forces
0
100
200
300
400
C-atom index

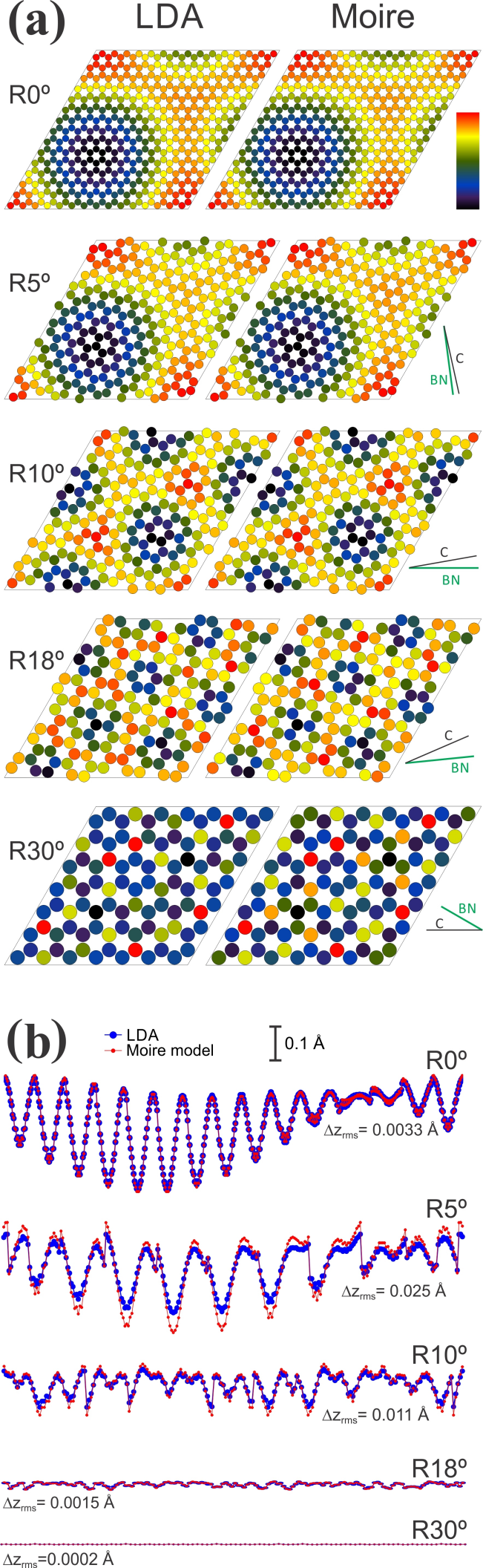
(a)
LDA
Moire
R0º
R5º
C
BN
R10º
C
BN
R18º
C
BN
R30º
BN
C
(b)
LDA
Moire model
0.1 Å
R0º
Δz_rms= 0.0033 Å
R5º
Δz_rms= 0.025 Å
R10º
Δz_rms= 0.011 Å
R18º
Δz_rms= 0.0015 Å
R30º
Δz_rms=0.0002 Å

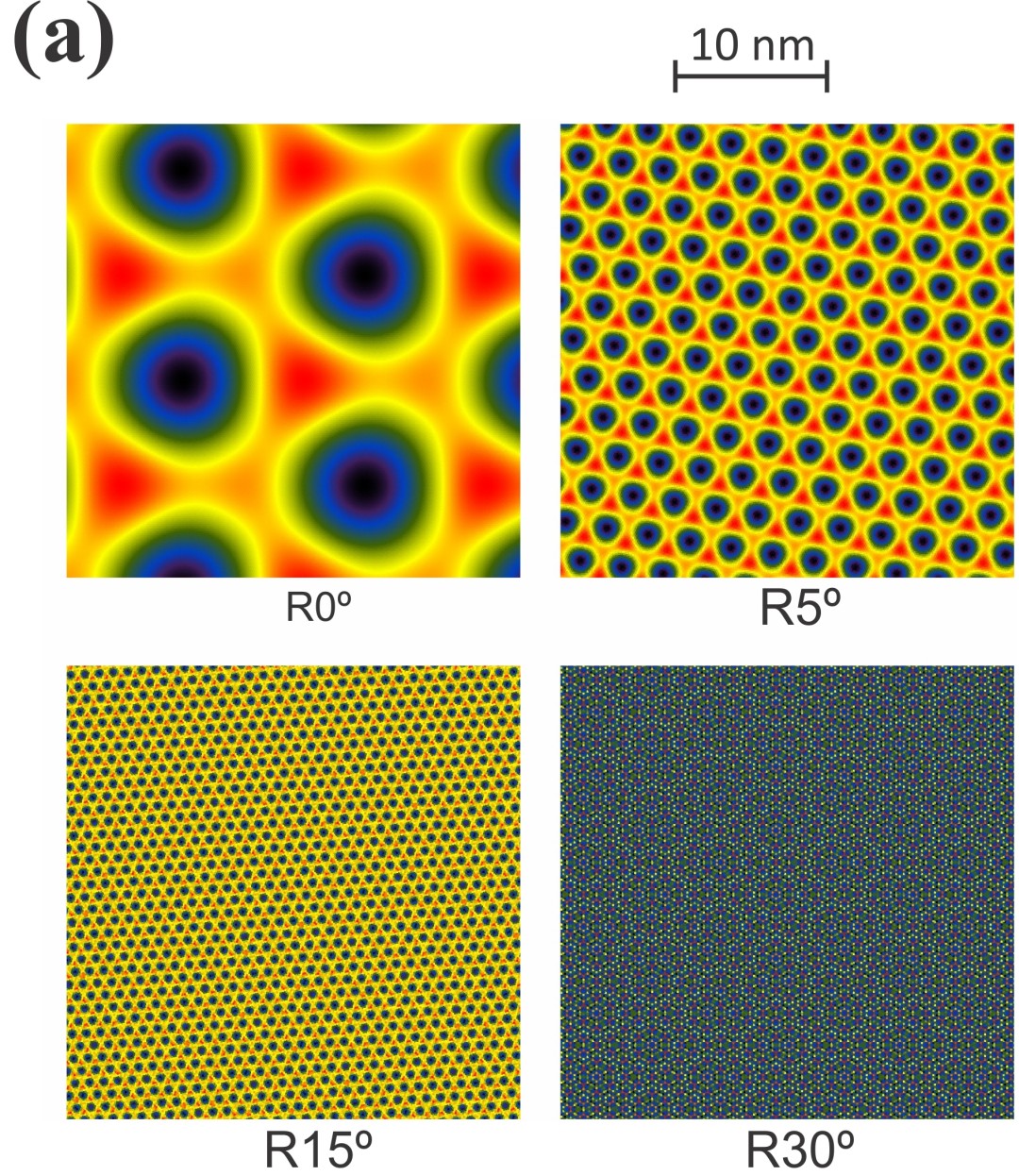
(a)
10 nm
R0º
R5º
R15º
R30º

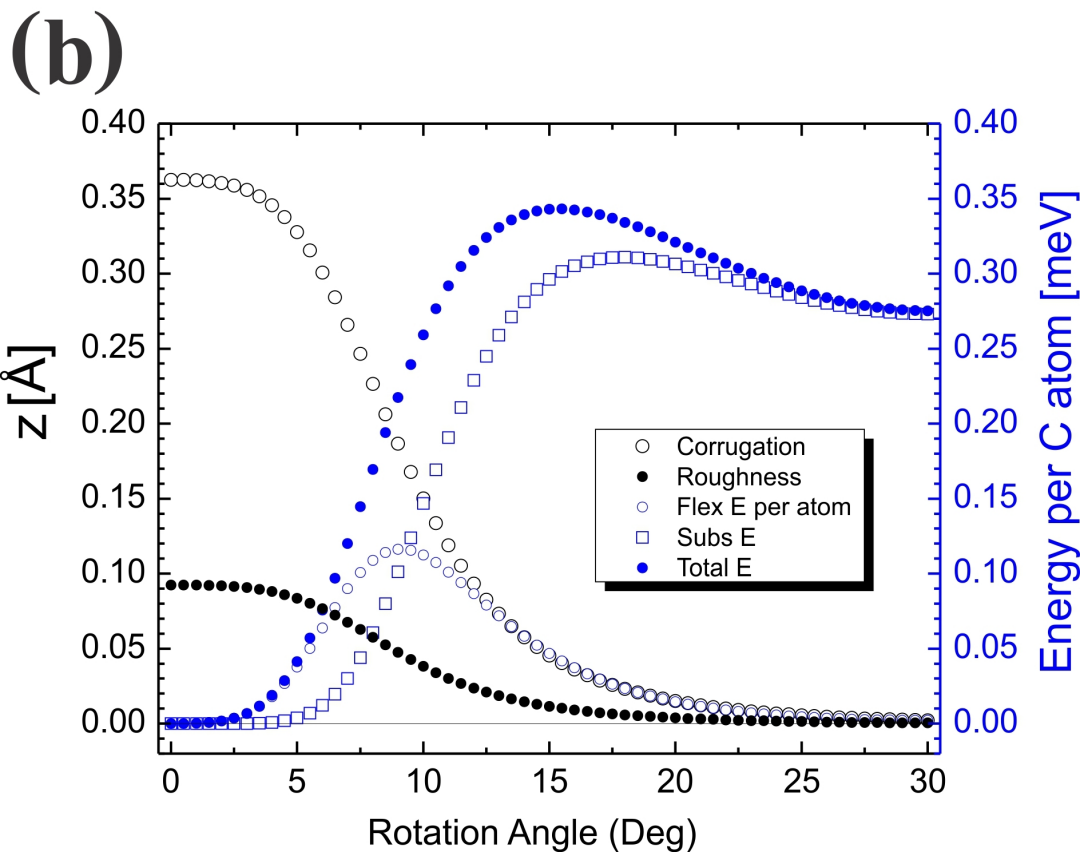
(b)
z [Å]
Energy per C atom [meV]
Rotation Angle (Deg)
Corrugation
Roughness
Flex E per atom
Subs E
Total E
0.00
0.05
0.10
0.15
0.20
0.25
0.30
0.35
0.40
0
5
10
15
20
25
30

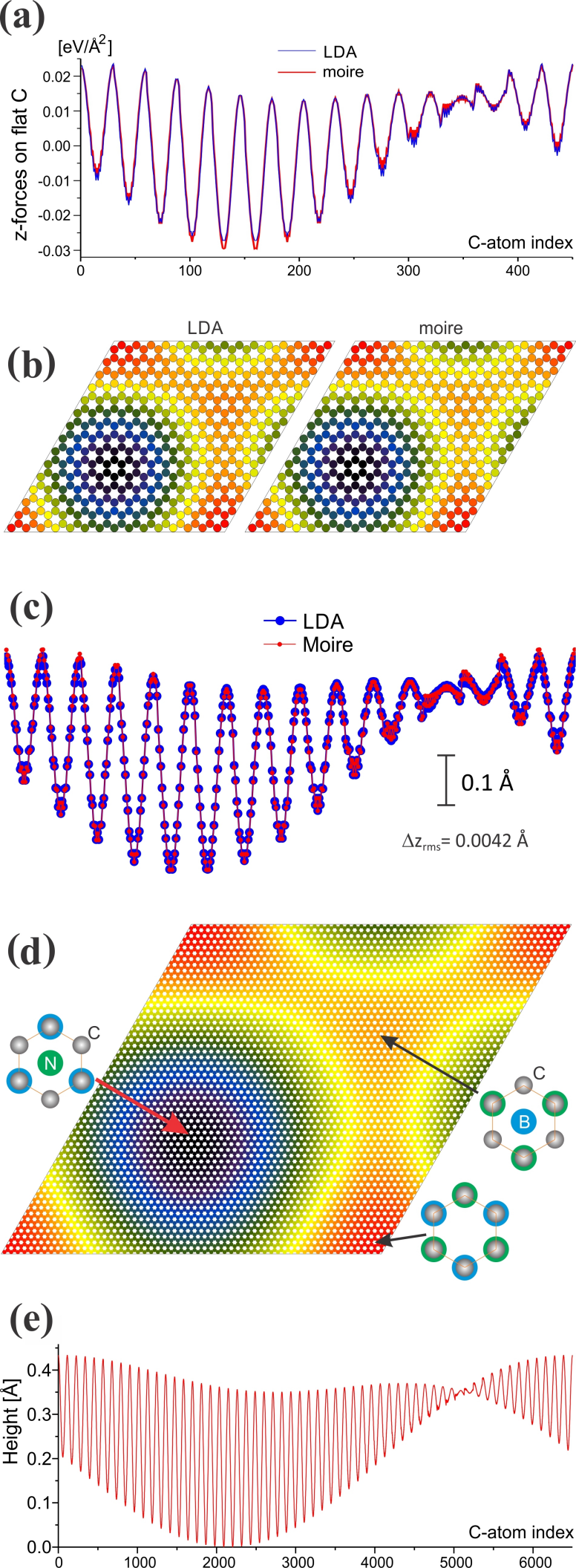
(a)
[eV/Å^2]
LDA
moire
z-forces on flat C
C-atom index
(b)
LDA
moire
(c)
LDA
Moire
0.1 Å
Δz_{rms}= 0.0042 Å
(d)
C
N
C
B
(e)
Height [Å]
C-atom index

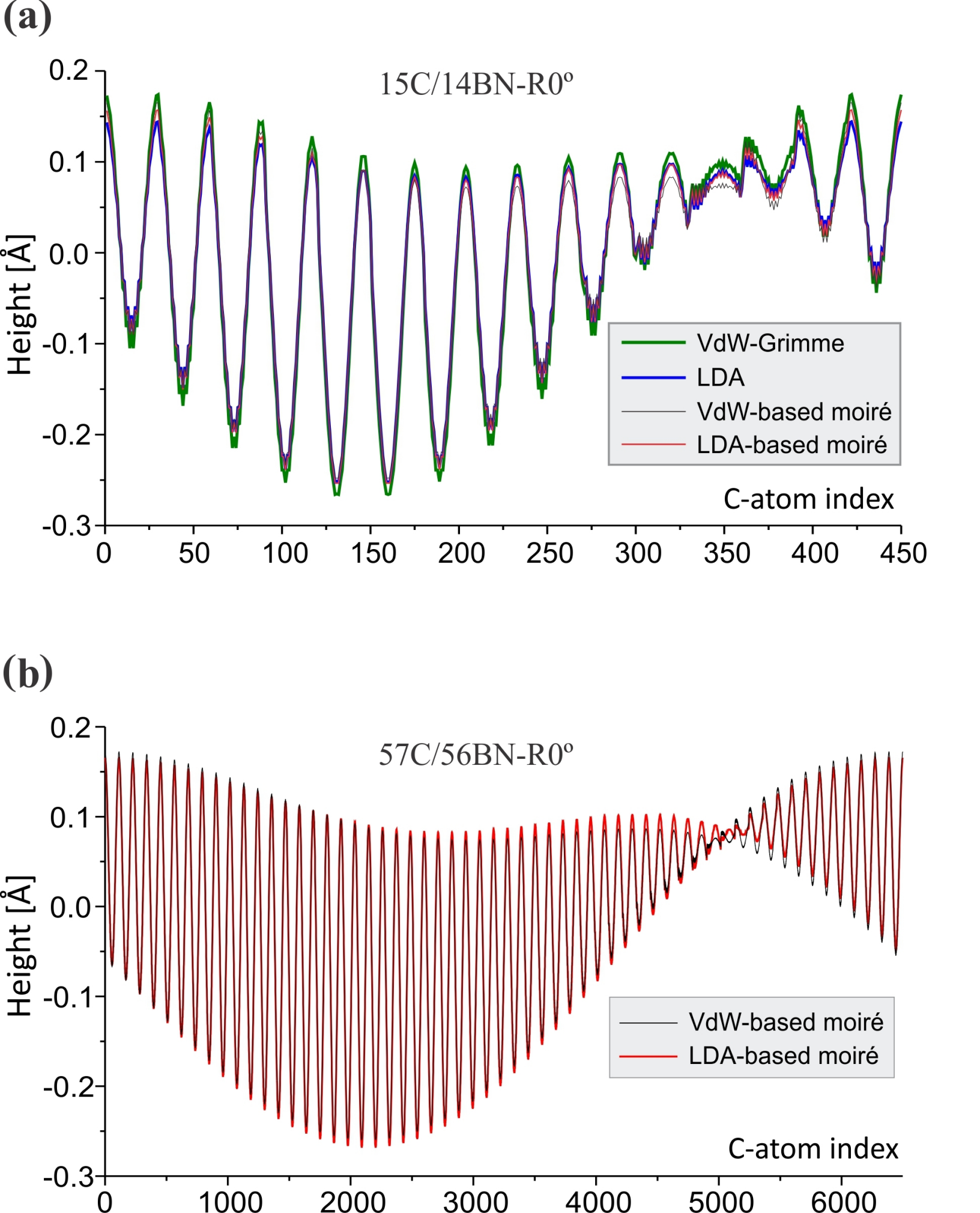
(a)
15C/14BN-R0º
Height [Å]
C-atom index
VdW-Grimme
LDA
VdW-based moiré
LDA-based moiré
0.2
0.1
0.0
-0.1
-0.2
-0.3
0
50
100
150
200
250
300
350
400
450
(b)
57C/56BN-R0º
Height [Å]
C-atom index
VdW-based moiré
LDA-based moiré
0.2
0.1
0.0
-0.1
-0.2
-0.3
0
1000
2000
3000
4000
5000
6000

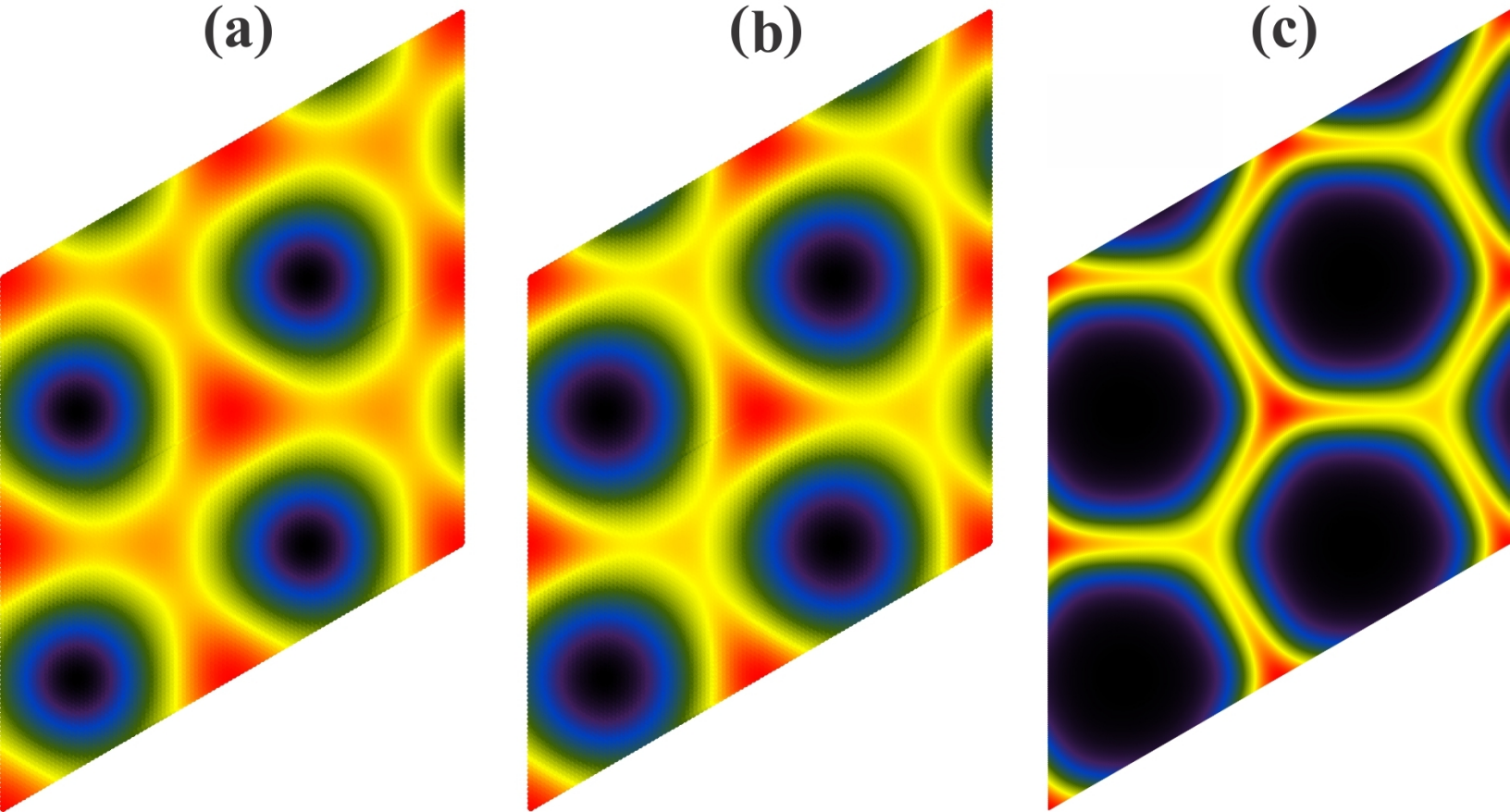
(a)
(b)
(c)